JOURNAL OF MATERIALS SCIENCE 31 (1996) 4483–4492

Influence of stress intensity and crack speed on fracture surface topography: mirror to mist to macroscopic bifurcation

D. HULL*
Department of Materials Science and Engineering, University of Liverpool, Liverpool, UK

The development of roughness on the fracture surfaces of a brittle, glassy, epoxy resin from the mirror-to-mist transition to macroscopic bifurcation has been investigated using optical microscopy, scanning electron microscopy (SEM) and contact and non-contact laser profilometry. Most of the observations were made on specimens fractured in edge-notched tension. In a series of tests the initial crack length was varied to obtain fracture surfaces formed by accelerating and decelerating cracks without macroscopic bifurcation (specimen A) and by cracks which accelerated continuously to macroscopic bifurcation (specimen B). Some observations were made on specimens tested in compact tension to study changes in fracture surface topography associated with crack arrest in stick-slip fracture. There was a close correlation between the topographical detail revealed by the different techniques. In specimen A the roughness increased progressively from the mirror-to-mist transition and reached a maximum before decreasing as the crack decelerated. The topographical features revealed by optical microscopy and SEM were the same for accelerating and decelerating cracks at the same roughness value. In specimen B the roughness increased continuously to macroscopic bifurcation. There was a close similarity between the topographical features at all levels of roughness. A simple model for the basic step involved in roughness formation is presented which involves an element of the crack tip tilting out of the plane of the main crack before stopping (micro-bifurcation). The scale of micro-bifurcation ranged from 3 μm in the early stages of mist, when the crack velocity was close to 10% of the shear wave velocity, to the full width of the specimen (6 mm) at macroscopic bifurcation. The micro-bifurcation process develops from crack surface undulations and does not involve micro-crack nucleating ahead of the main crack. It is concluded that the relationships between crack velocity and dynamic stress intensity, and the value of the limiting crack velocity, must be interpreted in terms of micro-mechanical processes at the crack tip which are strongly dependent on specific material characteristics.

1. Introduction

In a previous paper [1] the changes in surface topography at the transition from mirror to mist on the fracture surface of a brittle epoxy resin, tested in pure mode I, were described. It was shown that there was a sharp, though not discontinuous, change in surface roughness at the transition. Scanning electron microscopy (SEM) and atomic force microscopy (AFM) were used to determine the topographical changes which occurred at the transition. The main feature of the transition was the progressive development of surface undulations which eventually resulted in the formation of discrete steps (river line steps) parallel to the direction of crack propagation. Using Wallner line measurements it was shown that the crack velocity, v_c, at the transition was about 10% of the shear wave velocity, v_t, in the epoxy resin. It was noted that the sequence of events which occurred at the mirror-to-mist transition for an accelerating crack was the reverse of the sequence at the mist-to-mirror transition for a decelerating crack.

In this paper the full sequence of events associated with the development of mist from mirror-smooth fractures through to macroscopic bifurcation are described for the same epoxy resin used previously. It is usual, in the literature, to associate the later states of roughening after mist with the expression 'hackle fracture'. The definitions of mist and hackle appear to be purely arbitrary. To avoid confusion the term 'hackle' is not used in this paper except in reference to other work. Macroscopic bifurcation, on the other hand, is a clear cut and well-defined effect in which the main

* Emeritus Goldsmiths' Professor Metallurgy, University of Cambridge, U.K.

0022–2461

crack divides or branches so that a test sample separates into three or more parts. However, the mechanisms involved in macroscopic bifurcation closely resemble those which occur at an earlier stage of fracture and it is convenient to use the expression 'micro-bifurcation' for these effects.

The overall objectives and context of this work were outlined in the introduction to the first paper [1] and will not be repeated here, except to observe that there is, as yet, no clear understanding of the sequence of micromechanical events leading to surface roughening and bifurcation.

In the present experiments, in which the influence of the dynamic fracture toughness, K_d, and v_c, on the topography of cracks for the full range of crack velocities has been determined, we have used the work of Takahashi and Arakawa [2–4] to provide a basic frame-work for the experimental approach. In particular, we have used the same side-edge notched (SEN) plate geometry, which is illustrated in Fig. 1, and an epoxy resin which has similar mechanical properties. The most relevant features of the results from this test approach can be represented in the data shown in Fig. 2, which is taken from two papers by Takahashi and Arakawa [2, 4] (nb. although some of the data in the papers cannot be completely reconciled, because there is not sufficient information about the test parameters, the key features are valid). Both K_d and v_c were determined and the surface roughness, λ, defined in terms of the root mean square of roughness, R_q, (see previous paper [1]) was measured with a contact profilometer with a tip radius of 10 μm [4]. In this test geometry the overall fracture behaviour depends on the values of a_o and b_o. Takahashi and Arakawa used values of b_o between 10 and 30 mm. A sharp starter crack was used with $a_o = 8$ mm. The results in Fig. 2 are taken to be for a test with $b_o = 20$ mm although this is not stated explicitly except for the roughness measurements [4]. Initially, all three parameters, K_d, v_c and λ, increased rapidly with crack length and reached a maximum after the crack had grown beyond the loading line. The position of the peaks in Fig. 2 do not coincide and it was this observation that led to the suggestion [3] that surface roughness was best related

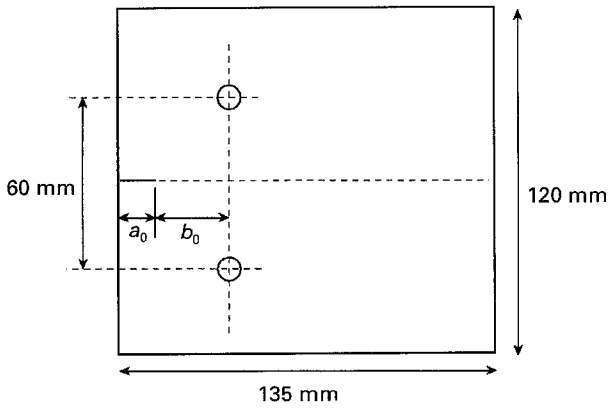

Figure 1 Shape and dimensions of edge-notched test specimens. Takahashi and Arakawa [2] used $a_o = 8$ mm and values of b_o between 10–30 mm. In the present work $(a_o + b_o) = 40$ mm and two values, $a_o = 10$ mm and $a_o = 15$ mm, were used.

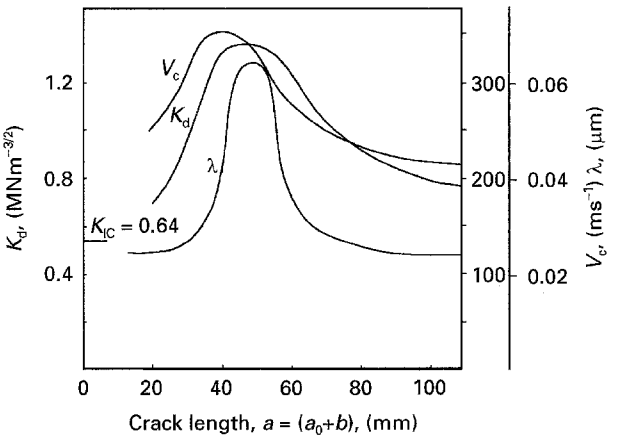

Figure 2 Summary of ENT data for a brittle epoxy resin, from Takahashi and Arakawa [2–4].

to fracture parameters by R^*v_c where

$$R^* = R_d - R_a = (K_d^2 - K_a^2)/E_d \quad (1)$$

R is the crack extension resistance and E is Young's modulus; subscript d relates to dynamic values and subscript a to the values for an arresting crack. The positions and heights of the peaks depended on the value of b_o. At large values of b_o the fracture load was low and fracture was smooth and continuous. At small values of b_o the fracture load was high and crack branching occurred. K_d at branching was about 4 MN m$^{-3/2}$ and the maximum or limiting value of v_c was about 400 ms^{-1} which is about 40% of the shear wave velocity. An important feature of the SEN test geometry is that the acceleration and deceleration of a crack can be investigated in the same test sample. The results in Fig. 2 indicate that K_d and λ are not the same for accelerating and decelerating cracks moving at the same speed.

The dimensions of the specimens used in work are shown in Fig. 1. These are closely similar to those used by Takahashi and Arakawa [2, 4] except that the plate thickness in this work was 6 mm rather than 5 mm. The dimension of $a_o + b_o$ was kept constant at 40 mm and different fracture responses were achieved by varying a_o. The results reported here are for specimens with two values of a_o, namely 15 mm and 10 mm. For $a_o = 15$ mm complete planar fracture occurred across the section and for $a_o = 10$ mm crack branching (macroscopic bifurcation) occurred. These specimens allowed a complete study of the fracture surface topography of (1) an accelerating and decelerating crack, and (2) a crack accelerating to branching.

Most of the details of the experimental methods and materials are the same as those described in the previous paper [1] and they are outlined only briefly in the next section. This is followed by a section on the development of surface roughness, in edge notch tension ENT and double torsion DT specimens, based on profilometry studies. In the next section there is a description of optical microscope observations which give an overview of the way that roughness increases progressively to macroscopic bifurcation. A simple model for the occurrence of roughness is

presented in the next section and details of SEM observations are described to support and develop the model to account for large scale roughness. The results are then discussed in the wider context of the influence of K_d and v_c on fracture surface topography in a range of materials.

2. Experimental methods and materials

The epoxy resin, described in the first paper [1], was used in this work. The test plates were about 6 mm thick. The properties of the resin are also given in the first paper.

Two mechanical test methods were used namely compact tension (CT), as described in the first paper, and edge-notched tension (ENT). As mentioned earlier the ENT test was based on the Arakawa and Takahashi test geometry with minor changes. The tests were made at $20 \pm 2\,^{\circ}C$ in a Schenck Universal testing machine with a cross head speed of 5 mm per min.

Roughness measurements were made with the Rodenstock non-contact laser profilometer, referred to in the previous paper, which has a 1 μm spot size. In addition a Taylor Hobson surface profilometer was used, as a check on the results from the Rodenstock instrument. This is a contact profilometer with a 2 μm stylus radius. Both profilometers were used to scan large parts of the fracture surface; details are given in later sections. The roughness parameter R_q, defined by

$$R_q = \left[\frac{1}{L}\int_0^L |f(x)|^2 \mathrm{d}x\right]^{1/2} \quad (2)$$

where L is the scanned length as $f(x)$ is the measured height of surface at point x, was used.

Optical and scanning electron microscopy was used as before [1] to investigate the topographical features.

3. Progressive development of roughness

Detailed measurements of roughness and observations of topographical features were made on two specimens tested using the ENT configuration, namely specimen A, with an initial crack length $a_o = 15$ mm which fractured at 1.8 kN, and specimen B with $a_o = 10$ mm which fractured at 4.4 kN. Specimen A fractured with a planar fracture, normal to the direction of applied load, completely across the specimen, without any macroscopic bifurcation. In specimen B macroscopic bifurcation occurred before the loading line and resulted in two separate curved fractures (Fig. 3a). The specimen fractured into three parts which were combined together for the photograph. Details of the micro-bifurcations, close to macroscopic bifurcation, are shown in Fig. 3b. An overview of one of the fracture surfaces showing the progressive increase in roughness up to macroscopic bifurcation is shown in Fig. 3c.

Roughness profiles were made on specimen A with the Rodenstock non-contact profilometer as illustrated schematically in Fig. 4a. The length of each scan was 5 mm and the measurements were made at

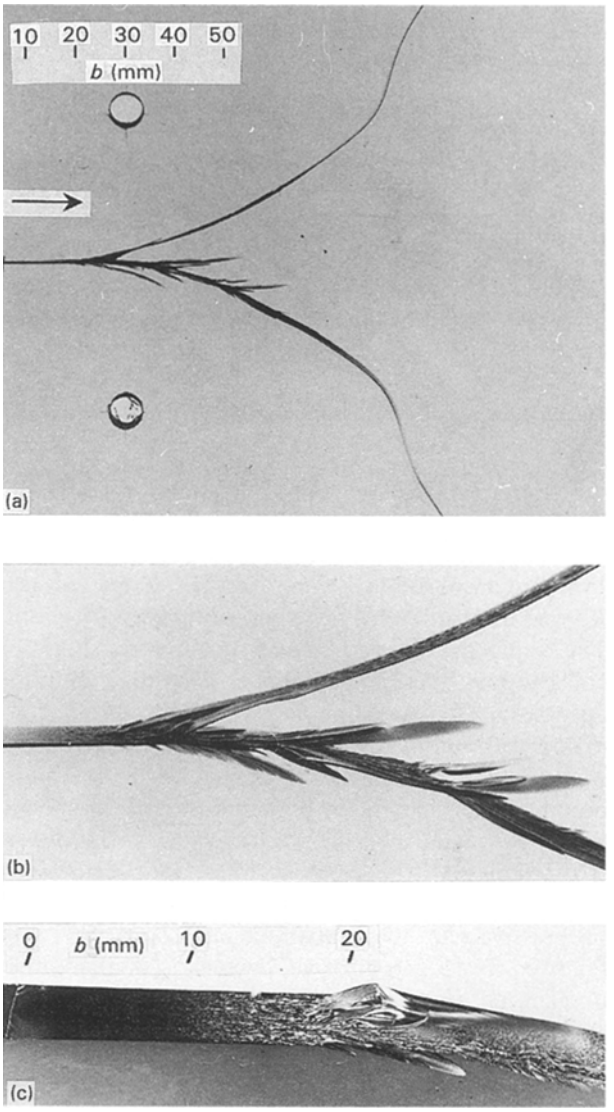

Figure 3 Optical photographs of macroscopic bifurcation in specimen B ($a_o = 10$ mm). (a) Overview showing position of bifurcation in relation to loading points; numbers refer to distance from nucleation (see Fig. 4). (b) Detail of macroscopic bifurcation region with extensive micro-bifurcation, (nb. specimen was tilted slightly to show cracks). (c) Fracture surface of lower part of specimen in (a) and (b) showing full range from nucleation to macroscopic bifurcation (branching) at $b = 20$ mm.

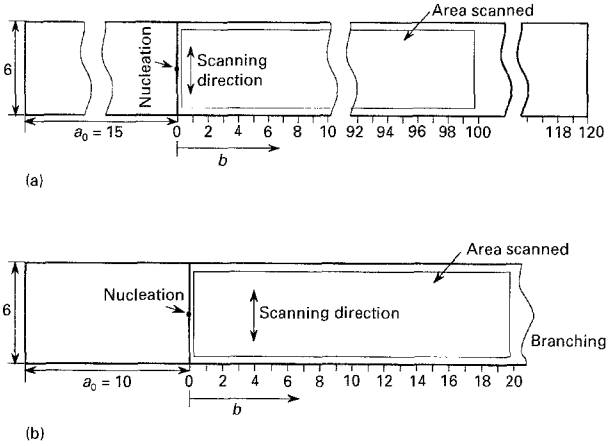

Figure 4 Illustration of regions examined by profilometry. (a) Schematic of specimen A. (b) Schematic of specimen B. Please note that all dimensions are in mm.

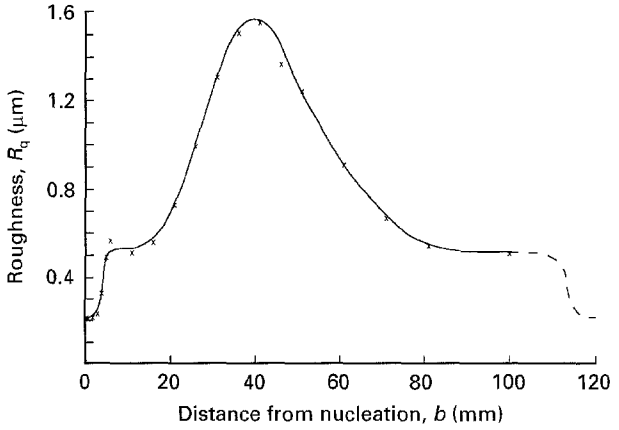

Figure 5 Variation of roughness with distance from nucleation on specimen A measured with Rodenstock non-contact laser profilometer.

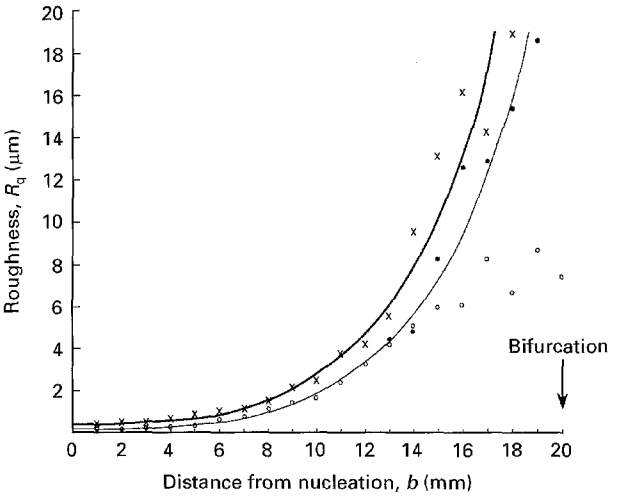

Figure 6 Variation of roughness with distance from nucleation on specimen B. (×) Rodenstock non-contact profilometer with scan length of 5 mm and cut off-lengths between 0.25–0.8 mm, (○) Hobson Taylor contact profilometer with scan length of 1.25 mm and 4 mm and cut-off lengths of 0.25 mm and 0.8 mm respectively, (●) Hobson Taylor contact profilometer with scan length of 4 mm and cut-off length of 0.8 mm.

1 mm intervals along 100 mm of the fracture surface. R_q was determined using a cut-off length of 0.2 mm. The results are shown in Fig. 5. In the early stages of crack growth the fracture surface was mirror smooth apart from a few river line steps which spread out from the nucleation point. In this region the roughness, R_q, was about 0.2 μm which is the same as the values obtained from the mirror region in the DT specimens reported previously [1] using the same profilometer. A sharp increase, to about $R_q = 0.55$ μm, occurred at the mirror-to-mist transition and then R_q increased progressively up to a maximum of 1.7 μm. This was followed by a progressive decrease, as the crack decelerated, and eventually, at the end of the crack, the surface became mirror smooth again. Because measurements were limited to $b = 0$–100 mm (Fig. 4a) the roughness in the final mirror region was not determined. However, it may be assumed that it was about 0.2 μm as indicated by the broken line in Fig. 5.

Roughness profiles were made on specimen B using both the Rodenstock laser profilometer and the Taylor Hobson contact profilometer. The details of the regions scanned by the Rodenstock profilometer are shown in Fig. 4b; the scan length was 5 mm. In determining R_q, a 0.25 mm cut-off length was used for b between 0–12 mm and a 0.8 mm cut-off length for the remainder of the fracture surface. The profilometer became unstable at $b = 18$ mm because the surface was too rough. Scans were made at 1 mm intervals. The results are shown in Fig. 6. Two sets of measurements were made with the Taylor Hobson profilometer and the values are also shown in Fig. 6. The R_q values shown by the open circles were obtained, with a 1.25 mm scan length and a 0.25 mm cut-off length, along the full length ($b = 0$ to 20 mm) of the central part of the fracture surface. The values shown by the closed circles were obtained, with a 4 mm scan length and a 0.8 mm cut-off length, for $b = 12$ to 20 mm. The distribution of the results and the apparent scatter are indicative of the problems of defining roughness. However, the overall pattern for both the Rodenstock and the Taylor Hobson profilometers is identical. The lower R_q values from the Taylor Hobson profilometer reflect the difference in the size of the probe. The scatter in these results at long crack

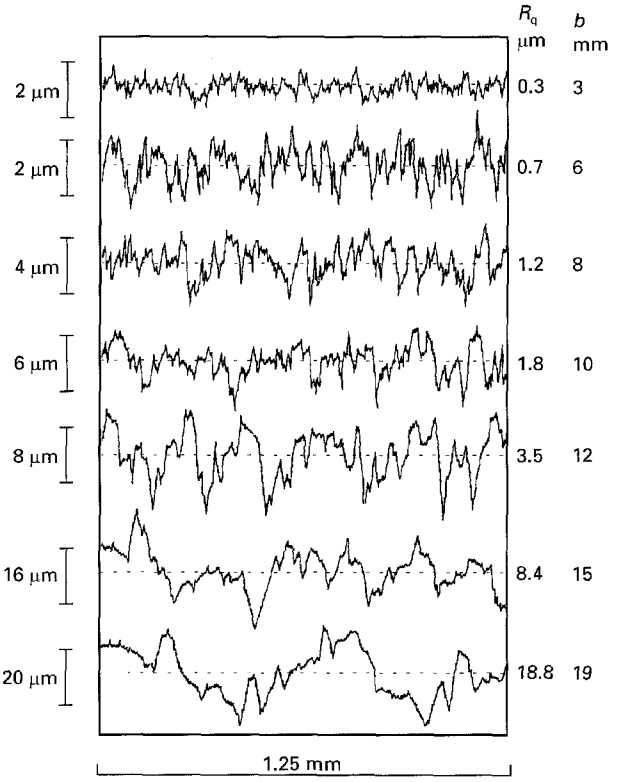

Figure 7 Selection of profiles of specimen B from Hobson Taylor profilometer illustrating the progressive change of scale as crack grows to macro-bifurcation.

lengths, particularly for the 1.25 mm scan length, arises because the scale of the roughness, and the dimensions of the fractographic features, are comparable to the cut-off dimension. This is illustrated by the selection of roughness profiles in Fig. 7. As b increased the overall scale of the roughness increased as indicated by the dimensional scales on the profiles. Both the height of the profiles and the horizontal scale of the roughness features increased progressively up to macroscopic bifurcation.

No mirror-smooth fracture occurred on specimen B except for a very small semi-circular region, less

than 0.1 mm diameter, which was closely associated with the nucleation process. Accordingly, no roughness measurements were made of this region. The value of R_q, determined with the Rodenstock profilometer, in the early stages of mist, was about 0.55 μm which corresponds to the value of R_q in the initial plateau for the mist region in specimen A. R_q increased continuously to macroscopic bifurcation and the maximum recorded value was about 20 μm.

Some roughness measurements were made also on the fracture surfaces of the compact tension (CT) specimens reported in the previous paper [1]. The CT tests were made, primarily, to determine K_{Ic}, the fracture toughness, of the resin. Some stick-slip fracture occurred but the overall fracture surface was very flat. The surfaces were mirror smooth, with isolated river line steps, except in the region of crack arrest and reinitiation. Here, additional roughness was generated by (i) small amounts of slow crack growth, (ii) local plastic blunting of the crack tip, leading to a higher K_I for crack initiation, and (iii) readjustment of the stress fields, all of which are outside the scope of this paper. Some typical slip-stick crack arrest boundaries are shown in Fig. 8a; note the direction of crack propagation. A higher magnification view of one of the boundaries is shown in Fig. 8b. The crack stopped at A–A and renucleated at a point site, outside the field of view (see Fig. 8c), before unzipping along the original crack front [5]. The initial stages of growth have a mist fracture surface. The mist-to-mirror transition at B–B′ between regions II and III is identical to the transition described in the first paper [1]. The isolated river line steps in region III eventually combined, as at C, or disappeared to produce a completely smooth and featureless surface.

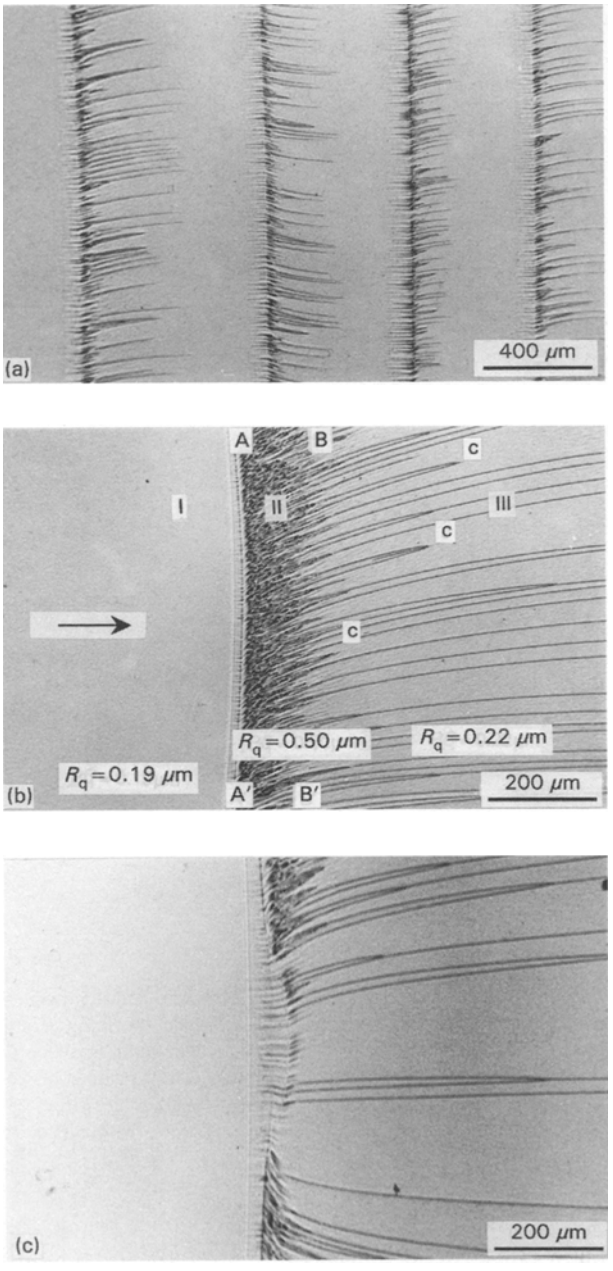

Figure 8 Optical microscope photographs of stick-slip crack arrest boundaries on fracture surface of compact tension specimen.

The roughness values, determined with the Rodenstock profilometer, with a 0.25 mm cut-off, were $R_q = 0.19$ μm in region I, $R_q = 0.50$ μm in region II, and $R_q = 0.22$ μm in region III. These results are consistent with all the previous data and confirm that in the mirror region R_q is constant and independent of the test configuration.

4. Optical microscope observations

Three general points can be made relating to observations on all the specimens tested in this work. (1) The topographical features at the transition from mirror-to-mist for an accelerating crack, and the mist-to-mirror transition for a decelerating crack, were the same as those described in the first paper for the double torsion specimen. (2) The sequence of changes and the development of topographical features for a decelerating crack were the reverse of the features for the accelerating crack. Thus, for example, referring to Fig. 5, the topographical details and dimensions of the fracture surface corresponding to $R_q = 0.8$ μm at $b = 22$ mm and 65 mm were essentially the same. (3) The sequence of changes associated with increasing roughness as the crack accelerated, and K_d increased, were identical in specimens A and B. In particular, the topography of specimen A at $R_q = 1.2$ μm, $b = 28$ mm and 52 mm was the same as in specimen B at $R_q = 1.2$ μm, $b = 7$ mm.

With these general points in mind it follows that the topographical features of progressive roughening from mist to macroscopic bifurcation can be observed on specimen B ($b = 0$ mm, $R_q = 0.5$ μm to $b = 20$ mm, $R_q \geqslant 20$ μm). An overview set of optical micrographs from this region is shown in Fig. 9. At this magnification the surface at $b = 2.5$ mm ($R_q = 0.55$ μm) appears smooth and uniform and it is easy to understand why it might be described as 'mist'. This surface corresponds to Fig. 5 in the first paper [1] but the magnification is lower and the optical conditions for photography were different.

As b increased, and v_c and K_d increased, the surface features became more pronounced. There is an element of scaling with a close correlation between the topographical dimensions in Fig. 9 and the dimensions and spacing of the serrations in Fig. 7 at the corresponding values of b. Detailed microscopic

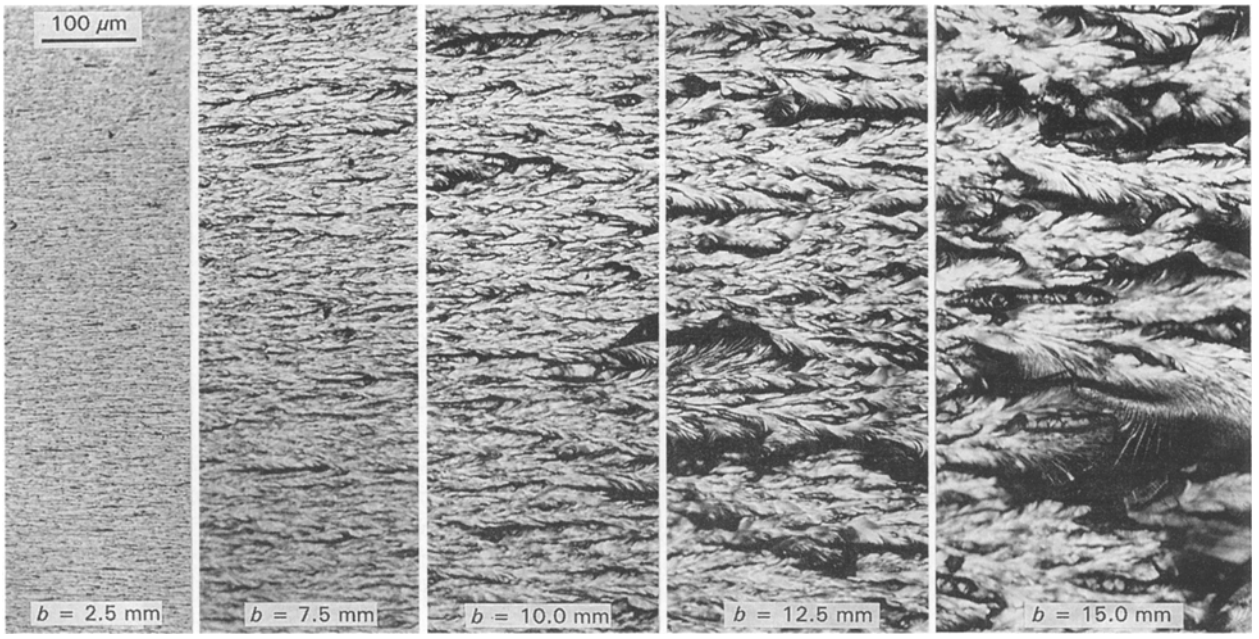

Figure 9 Optical microscope photographs, all at the same magnification, at different positions along the fracture surface of edge-notched tensile specimen B.

examination revealed that the same topographical features occurred throughout the whole range from mist to macroscopic bifurcation.

A major feature at all magnifications, described in more detail in the next section, was the local tilting of the crack front out of the plane of the main crack to form semi-elliptical shape features which are, in essence, micro-bifurcations. The optical photographs in Fig. 9 demonstrate that the scale of these features increased with b and, additionally, that small scale features were superimposed on the large scale features.

5. Interpretation of topography using additional SEM observations

To assist in the description of the topography we now propose a simple model based on all the observations which have been made in this work. Fig. 10 shows an idealized form of the basic unit feature on the fracture surface. The propagating crack, undulating as described in the first paper [1], develops 'river line' steps in the manner demonstrated by the atomic force microscope data in Fig. 18 of reference [1]. Suppose that two steps, of opposite sign and of the same height, are formed simultaneously at the expanding crack tip at positions N_1 and N_2. The element of crack front between the two steps then tilts out of the plane of the main crack. The shape of the tilted region, in a section parallel to direction of main crack propagation, is shown in Fig. 10b and may be inferred from the shape of large tilted cracks (Fig. 3). The tilted crack then interacts with the main crack along N_1M_1 and N_2M_2 and then the separated cracks tilt towards each other leading to the formation of filaments of material parallel to N_1M_1 and N_2M_2. Eventually the tilted crack stops and this leaves fork-shaped filaments, which are joined to both surfaces of the main crack, and a characteristic semi-elliptical feature on the fracture surface.

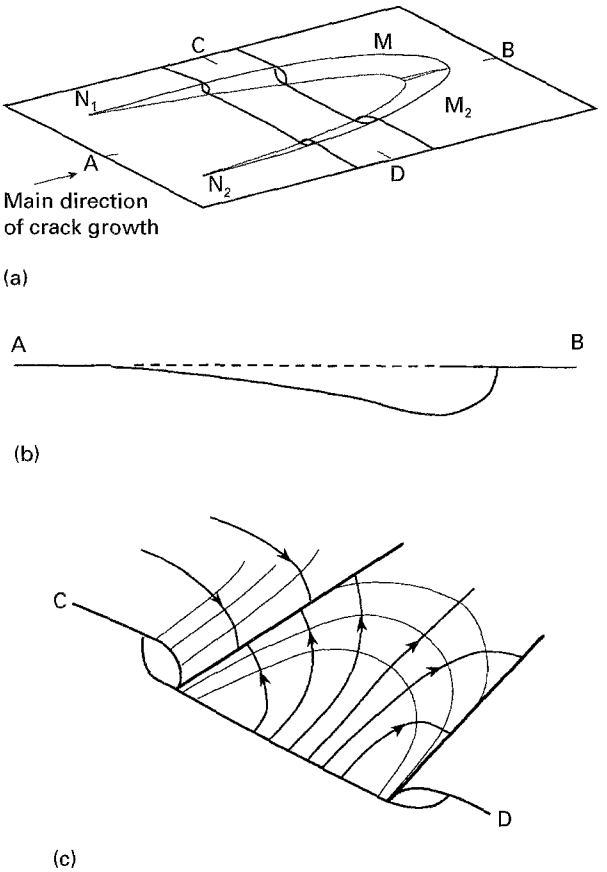

Figure 10 Schematic representation of formation and growth of micro-bifurcation. (a) Basic unit feature formed by tilting of element N_1N_2 of crack front. (b) Section A–B illustrating shape of tilted elements. (c) Local crack growth directions in region of section C–D; thick lines with arrow heads show crack growth directions, fine fines show successive positions of crack front which are normal to crack growth directions.

As the crack opens the filaments, which bridge the main crack, break off leaving debris on the fracture surface, some of which remains attached to one or other of the fracture surfaces.

The local directions of crack growth, represented in the schematic in Fig. 10c, show the way that the crack expands in the region of the tilted elements. As we shall see later, some of the crack movements cannot be achieved fully by tilt movements and local mixed mode I/III stress fields are generated. These lead to a series of river line steps of the same sign and characteristic river line patterns [6]. Similarly, at high K_I, when the tilted elements are large, the processes are repeated on a smaller scale on the individual elements.

The simple model, illustrated in Fig. 10, requires modification in the real world. Thus, for example, the steps may not be of the same height, they may not form simultaneously and they may not be of opposite sign. Also, the individual steps may smooth off into surface undulations instead of meeting each other, particularly for decelerating cracks. These 'chaotic' aspects lead to a whole variety of surface features which are evident on the fracture surfaces. Some of these, but by no means all; will be identified by

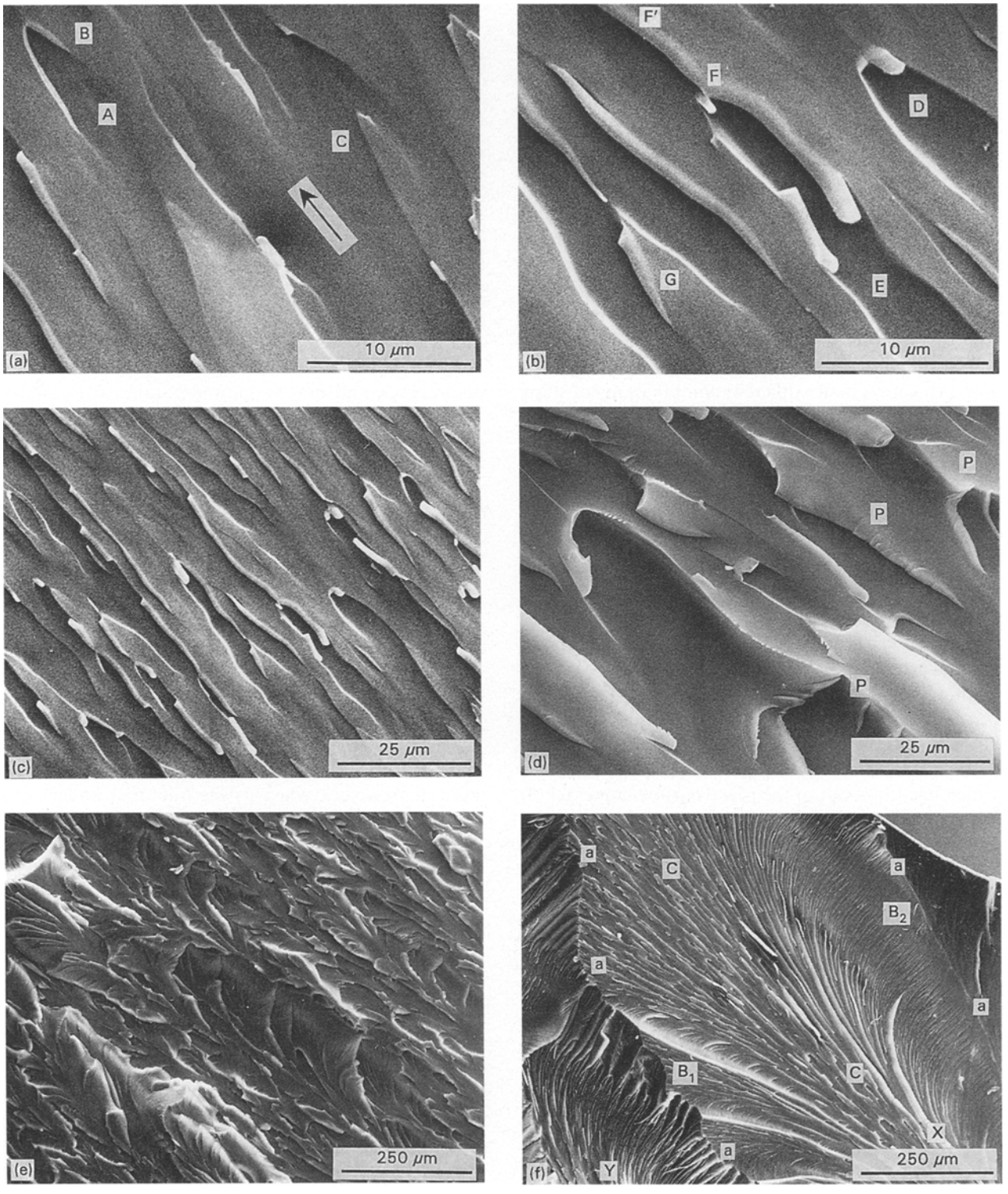

Figure 11 SEM photographs at different positions along the fracture surface of edge-notched tensile specimen B. (a) Early stage of mist ($b = 1.0$ mm, $R_q = 0.55$ μm). (b) ($b = 2.5$ mm, $R_q = 0.6$ μm). (c) Same region as Fig. 11b at lower magnification. (d) ($b = 6$ mm, $R_q = 1$ μm). (e) ($b = 12$ mm, $R_q = 5$ μm). (f) Close to macroscopic bifurcation; two large 'micro-bifurcations' showing pure mode I and mixed mode I/III fractographic features and many superimposed micro-bifurcations at different scale levels.

reference to SEM photographs. They are evident also in the optical microscope photographs.

Examples of the elementary units (Fig. 10) from the early stages of mist are shown in Fig. 11a ($b = 1$ mm, $R_q = 0.55$ μm). At A a symmetrical set of steps of opposite sign have been nucleated and there are residual filaments on the fracture surface. The element of the crack front between the steps has tilted away (downwards) from the main fracture plane before terminating at B. The same feature is shown at C except that this represents the opposite face of the fracture to the feature at A, i.e. the crack element has tilted upwards. Thus, A and C show the appearance, on opposite fracture surfaces, of the same (equivalent) element of crack tilting out of the main plane of the crack. It follows that Fig. 11a shows elements which have tilted upwards and downwards in close proximity.

The surface steps are more pronounced in Fig. 11b ($b = 2.5$ mm, $R_q = 0.6$ μm). An approximately symmetrical tilt region is shown at D with part of the filaments on the surface. The rest of the filaments had broken off or were attached to the opposite fracture surface. At E two steps of opposite sign but of unequal height have joined leaving a residual step of one sign along FF′. An example of the equivalent feature on the opposite fracture surface is shown at G. A lower magnification photograph (Fig. 11c) of the same region as Fig. 11b shows many different combinations of steps.

As the crack length increased the features became progressively more pronounced (Fig. 11d, $b = 6$ mm, $R_q = 1$ μm). Additional details of the way that tilted crack elements join together are shown at P. This complexity increased as b increased (Fig. 11e, $b = 12$ mm, $R_q = 5$ μm). The tilted crack elements were much larger and there was considerable fine detail surface topography in each element which resulted from a complex mixture of local mixed-mode loading and K_d effects. Detail from two such elements is shown in Fig. 11f. One crack element has formed from region X and the other from region Y. This relatively low magnification photograph was taken close to the region where crack branching occurred ($b = 20$ mm). The region marked by (a–a–a) is a crack which has tilted out of the plane of the main crack. It shows two quite distinct topographical features. The narrow central band C–C has a topography similar to that shown in Fig. 11c, which was produced by an overall mode I loading condition. The outer areas, B_1 and B_2, have well-defined river line steps of the same sign which is characteristic of mixed mode I/III fracture [6]. The interpretation of these features is considered briefly in the next section. The mode I/III steps result in a whole series of crack fronts and these features are repeated again on a finer scale on these coarse crack fronts. The orientations of the markings in region (a–a–a) are consistent with the directions of crack movements and the positions of the expanding crack fronts illustrated in Fig. 10c.

6. Concluding discussion

We have established already [1] that in this brittle epoxy resin material the mirror to mist transition occurs at $v_c \cong 0.1\, v_t$. We return later to the significance of this in relation to other materials. Since the geometry and dimensions of the test samples were based on those used by Takahashi and Arakawa's work [2–4], and the properties of the epoxy resin were similar, it seems reasonable to relate the data produced in the two sets of experiments. They reported that macroscopic bifurcation occurred at $v_c \cong 0.4\, v_t$ and so this provides an upper limit to the crack velocity. Apart from the Wallner line and related measurements reported in the first paper [1] no other means of determining crack velocity was used in the present work and one can only infer, from other observations, the velocities of the crack which generated the topographical features. The lack of a direct correlation between v_c and λ (R_q) shown in the Takahashi and Arakawa data (Fig. 2) means that such inferences may be suspect. However, there is much evidence in the data generated in this work that, in the crack acceleration stage, after the mirror-to-mist transition, the crack velocity increased very rapidly with only a small increase in surface roughness and presumably only a relatively small increase in K_d.

A fundamental conclusion from the observations in this work is that the roughness is generated by elements of the main crack tilting out of the plane of the main crack and not by the nucleation of secondary cracks ahead of the main crack. The discrete tilting events were preceded by the development of surface undulations and occurred first at $v_c \cong 0.1\, v_t$. The tilting process was associated with the nucleation of the surface steps. There was no evidence, on the scale of the undulations or the step spacing, for any microstructural involvement. This observation is entirely consistent with those reported previously for surface steps generated in mixed mode I/III [6]. There is undoubtedly experimental evidence in some materials for surface roughness derived from the nucleation of secondary cracks ahead of the main crack front, notably the occurrence of parabolas in PMMA and other thermoplastics: (nb. parabolic markings were present on the fracture surfaces of the epoxy resin used in this work when it was fractured under conditions which favoured increased toughness such as increased temperature or a different set of curing conditions).

The most substantial case in favour of roughness being the result of the nucleation of secondary cracks ahead of the main crack tip is offered by Ravi-Chandar and Knauss [7] as part of a series of important papers on dynamic fracture [7–10]. Indeed many of the observations in the present work are closely similar to those reported by Ravi-Chandar and Knauss [7] and it is important to recognise the value of this seminal work. However, Ravi-Chandar and Knauss [7] concluded that: "In the "mist" zone, the crack propagates at higher stress intensities compared to the "mirror" zone. Here, the stresses ahead of the crack front are high enough to initiate and then grow the voids prior to the arrival of the main crack front". The material used by Ravi-Chandar and Knauss was Homolite-100 which is a brittle cross-linked polyester

resin with many property characteristics similar to the epoxy used in the present work. There can be no doubt that existing voids can grow and interact with the crack front but the concept of voids acting to develop secondary cracks down to the scale of a few micrometres, as evident in the early stage of mist, Fig. 11, is far from being established. Indeed, it seems likely that most of the Ravi-Chandar and Knauss observations on micro-branching have the same interpretation as those presented in this paper which require that micro-branching is achieved by the expansion of small elements of the crack front out of the primary plane of crack growth rather than involving secondary crack nucleation. Some of the other topographical observations reported by Ravi-Chandar and Knauss are consistent with, and may be explained by the approach used in this paper. It is also worth noting that recent models of dynamic crack growth, such as those offered by Rice *et al.* [11] and Gao [12] may eventually offer a basis for rigorous explanations of the phenomena described in this work but, at present, they have many limitations, well understood by these authors.

The scale of the topographical features and the roughness increased with v_c and K_d and there is some scope for applying fractal analysis, but this was not an objective of the present work. The upper limit to the scaling occurred at macroscopic bifurcation or crack branching, which, in turn, determined the limiting crack velocity. The observations showed clearly that macroscopic bifurcation occurred when the dimensions of the tilted crack elements approached the thickness of the test sample, because it is only then that the crack could 'escape' from the main plane in which it was propagating. The tilting of small elements at $v_c \cong 0.1\, v_t$ is equivalent to full scale branching except that the crack cannot 'escape' because the lengths of the elements are small compared with the thickness of the plate (3 μm compared with 6 mm). Thus, the crack was constrained to the main path of fracture, normal to the applied stress, by the stabilizing effect of multiple elemental cracks of opposite sign. At crack branching the cracks reached the dimensions of the plate. It follows that the critical condition for macroscopic bifurcation is dependent on simple geometrical factors, such as the thickness of the plate. It then seems unreliable to relate bifurcation to a critical crack velocity. These observations have a considerable bearing on the validity of continuum mechanics models currently used to explain roughness and bifurcation (see reference [13] for a review). Clearly, the velocity at the mirror-to-mist transition cannot be related directly to the predictions of stress field rotation, associated with inertial effects, as first developed by Yoffe [14].

The fracture topography is also strongly affected by geometrical rules [15]. For a perfectly elastic crack the movements associated with the formation of undulations at the start of the mirror-to-mist transition and the development of the semi-elliptical features, idealized in Fig. 10, are severely restricted by the condition that a crack cannot twist. This leads to the development of local mixed-mode I/III conditions, even though the main crack is being driven by pure mode I loading conditions. Many of the features observed are the same as those described in reference [6]. The result of a multiplicity of individual crack-tilting events (Fig. 10) involving the creation of mixed mode I/III stress fields and a highly complex array of crack fronts must be taken into account in any realistic model for the expanding crack tip. The total area of fracture will be much increased by the development of roughness, through a whole range of scales, and the local crack tip velocity will vary widely. In each tilted element the crack velocity will be high initially and drop to zero at the end of the tilt around the boundaries of the two sets of cracks which have tilted towards each other as a result of elastic interactions.

As mentioned in the introduction, it is customary to refer to the very rough surfaces, which precede macroscopic bifurcation, by the term 'hackle'. This implies that a significantly different process is involved in the later stages of crack growth which the present results show, is clearly not the case. There are some fracture test geometries in which the expanding crack front has a pronounced curvature, as, for example, in tensile tests of round bars with a surface nucleated crack. The geometrical rules mean that such cracks cannot undergo macroscopic bifurcation on a continuous crack front. This results in roughness features, distinct from those generated by a straight crack front, which are more appropriately termed 'hackle'.

These results also have a bearing on the long-standing discussions about the limiting velocity of cracks and the relation between v_c and K_d in 'brittle' solids. It seems that there is a need for a re-evaluation of the evidence from a wide range of solids. Simple models for perfectly elastic solids indicate that, in a simple dead-loading tensile test, neglecting inertial effects, v_c should increase to the terminal velocity instantaneously as soon as a crack is initiated, so that the v_c–K_d relationship is discontinuous. Because of experimental difficulties measurements of v_c–K_d have been limited, largely, to transparent thermoplastics such as PMMA (e.g. Plexiglas) and thermosets such as polyester resins (e.g. Homolite-100) and epoxy resins (e.g. Araldite) [16]. The results show that, initially, v_c increases rapidly with only a very small increase in K_d and then levels off at a terminal velocity below that predicted by conventional inertial arguments. The reason for the difference between predictions for a perfectly elastic solid and these experimental observations relate to material effects and, in particular, to crack tip effects. Thus, for example, the fracture behaviour of PMMA is dominated by crazing, which is a pre-cursor of crack growth, so that many of the characteristics of fracture are determined by the mechanics and kinetics of crazing [17]. Where crazing is suppressed and the crack is constrained to move in a plane, as in the experiments of Washabaugh and Knauss [18], crack speeds approaching the terminal velocity, predicted by conventional arguments, have been recorded. Similar results have been obtained in the cleavage of crystals where the crack is constrained by interatomic force considerations and dislocation movement is minimized by a high Peierl's

force. Thus, for example, in the cleavage fracture of tungsten single crystals at 20 K, with atomically sharp pre-cracks introduced by spark cracking, crack velocities reaching 0.82 v_t have been recorded [19]. The fracture surfaces were mirror smooth at these crack velocities. Similar high velocities have been reported in other single crystals such as magnesium oxide, diamond and sapphire [20].

In the development of roughness in the fracture of crystalline solids there is ample evidence to suggest that micro-mechanical effects such as slip (dislocation glide), mechanical twinning, and interface de-cohesion may contribute. In some cases these effects result in micro-cracking ahead of the main crack tip and in other cases, as in the present experiments on a brittle epoxy resin, these effects lead to roughness by direct expansion of the main crack tip. The importance of local crack tip effects, which are strongly material-dependent, in evaluating the relation between v_c and K_d, and in predicting the limiting crack velocity, in all brittle solids, cannot be over-emphasised.

Acknowledgements

The author acknowledges the help with profilometry from Dr. Glyn Roper, Shell Thornton Research Laboratories, and with scanning electron microscopy from Dr. Peter Beahan, Liverpool University. Valuable discussions were held with Dr. Elizabeth Yoffe, Cambridge University and Professor K. Takahashi, Kyushu University. Professors Peter Goodhew and David Bacon and their colleagues are thanked for allowing the author to work in their Department at Liverpool University.

References

1. D. HULL, *J. Mater. Sci.* **31** (1996) 1829.
2. K. TAKAHASHI and K. ARAKAWA, *Expt. Mech.* **44** (1987) 195.
3. *Idem, Int. J. Fract.* **48** (1991) 103.
4. *Idem, Photomechanics and Speckle Metrology* **814** (1987) 670.
5. D. HULL, *Int. J. Fract.* **66** (1994) 295.
6. *Idem, ibid.* **70** (1995) 59.
7. K. RAVI-CHANDAR and W. G. KNAUSS, *ibid.* **26** (1984) 65.
8. *Idem, ibid.* **25** (1984) 247.
9. *Idem, ibid.* **26** (1984) 141.
10. *Idem, ibid.* **26** (1984) 189.
11. J. R. RICE, Y. BEN-ZION and K. S. KIM, *J. Mech. Phys. Solids* **42** (1994) 813.
12. H. GAO, *ibid.* **41** (1993) 457.
13. L. B. FREUND, "Dynamic fracture mechanics" (Cambridge University Press, Cambridge, 1990).
14. E. H. YOFFE, *Phil. Mag.* **42** (1951) 739.
15. D. HULL, *Int. J. Fract.* **62** (1993) 119.
16. J. W. DALLY, W. L. FOURNEY and G. R. IRWIN, *ibid.* **27** (1985) 159.
17. B. COTTERELL, *ibid.* **4** (1968) 209.
18. P. D. WASHABAUGH and W. G. KNAUSS, *ibid.* **65** (1994) 97.
19. D. HULL and P. BEARDMORE, in Proceedings of the First International Conference on Fracture, Sendai, 12–17 September 1965, edited by T. Yokobori, T. Kawasaki, J. L. Swedlow (Japan Society for Strength and Fracture of Materials, Sendai, 1966) Vol. 2, pp. 629–645.
20. J. E. FIELD, *Contemp. Phys.* **12** (1971) 1.

Received 3 January 1996
and accepted 15 January 1996